Nationaal Lucht- en Ruimtevaartlaboratorium
National Aerospace Laboratory NLR

NLR TP 96082

Four-stream atmospheric correction model

W. Verhoef

DOCUMENT CONTROL SHEET

	ORIGINATOR'S REF.		SECURITY CLASS.
	NLR TP 96082 U		**Unclassified**

ORIGINATOR
National Aerospace Laboratory NLR, Amsterdam, The Netherlands

TITLE
Four-stream atmospheric correction model

PRESENTED AT

AUTHORS	DATE	pp	ref
W. Verhoef	**960209**	**37**	**13**

DESCRIPTORS

Atmospheric correction
Atmospheric effects
Atmospheric models
Atmospheric optics
Atmospheric scattering
Bidirectional reflectance
Imaging techniques
Infrared absorption
Rayleigh scattering
Satellite imagery
Thematic mappers (Landsat)

ABSTRACT
This report describes some methods of correction for atmospheric effects on multispectral images acquired by earth observation satellites like Landsat. The effects of the atmosphere on optical images of the earth's surface are described by means of a four-stream radiative transfer model and the parameters of this model are derived on the basis of atmospheric optical properties like the optical thickness, the single scattering albedo and the scattering phase function of the major constituents air molecules and aerosol particles. Also the effect of gaseous absorption of radiation by water vapour and ozone can be incorporated in this yet relatively simple model. Making use of several relationships reported in the literature, the determination of unknown properties of the atmosphere can be reduced to estimation of the aerosol optical thickness and several methods to derive this quantity from measurements and images are discussed. One of these methods is the so-called "darkest pixel" method and some results of applying this method to Landsat Thematic Mapper data are presented.
The results indicate that by means of calibration of the satellite data and subsequent atmospheric correction it is possible to generate images of the multispectral surface reflectance in all optical Thematic Mapper bands. The derived surface reflectances have been compared with concurrent measurements on the ground in one case and to NIWARS field spectrometer data in another. From these comparisons it is concluded that in the near and mid-infrared in some cases the effect of water vapour absorption is underestimated and that the modelling of the so-called "adjacency effect" should be improved when a higher accuracy is required.

Summary

This report describes some methods of correction for atmospheric effects on multispectral images acquired by earth observation satellites like Landsat. The effects of the atmosphere on optical images of the earth's surface are described by means of a four-steam radiative transfer model and the parameters of this model are derived on the basis of atmospheric optical properties like the optical thickness, the single scattering albedo and the scattering phase function of the major constituents air molecules and aerosol particles. Also the effect of gaseous absorption of radiation by water vapour and ozone can be incorporated in this yet relatively simple model.
Making use of several relationships reported in the literature, the determination of unknown properties of the atmosphere can be reduced to estimation of the aerosol optical thickness and several methods to derive this quantity from measurements and images are discussed. One of these methods is the so-called "darkest pixel" method and some results of applying this method to Landsat Thematic Mapper data are presented.
The results indicate that by means of calibration of the satellite data and subsequent atmospheric correction it is possible to generate images of the multispectral surface reflectance in all optical Thematic Mapper bands. The derived surface reflectances have been compared with concurrent measurements on the ground in one case and to NIWARS field spectrometer data in another. From these comparisons it is concluded that in the near and mid-infrared in some cases the effect of water vapour absorption is underestimated and that the modelling of the so-called "adjacency-effect" should be improved when a higher accuracy is required.

Contents

2 Tables
9 Figures

(37 pages in total)

1 Introduction

In this report the effect of the atmosphere on optical remotely sensed images is described by means of four-stream radiative transfer theory. For the atmosphere, approximate extinction and scattering coefficients are derived based on aerosol scattering, Rayleigh scattering and absorption by water vapour and ozone gas. These are subsequently applied in order to obtain the reflection and transmission properties of the atmospheric layer. By means of the adding method the bidirectional reflectance of the combination atmosphere - earth's surface can be found. This quantity is also called planetary reflectance and the signal detected by earth observation satellites in the 'optical' window (0.4 - 2.5 μm) is directly proportional to it.

Atmospheric correction is the derivation of the reflectance of the earth's surface from the planetary reflectance. This can be useful for radiation budget studies and for a better spectral characterization of objects on the ground. The conditions under which atmospheric correction can be carried out successfully are limited, however. The main requirements are that the atmosphere is laterally homogeneous, its constituents are known, and that the earth reflectance can be approximated as being Lambertian.

Since in most cases the concentrations of some atmospheric constituents, such as water vapour and aerosol, are not known, one usually applies techniques to estimate these quantities from the imagery or from meteorological observations. The less variable effects, such as Rayleigh scattering, are described in the literature and can easily be included in atmospheric models.

2 Description of the atmospheric effect

The effect of the atmosphere on satellite observations of the earth is illustrated in figure 1. Here one can identify three contributions to the radiance detected by the satellite: 1) a contribution from the target illuminated by direct sunlight and diffuse skylight and 2) a contribution caused by scattered sunlight and 3) a contribution from objects outside the field of view. The latter two contributions together form the so-called path radiance, in which 2) is the atmospheric part and 3) the "background" part. The background contribution is said to be caused by the "adjacency"-effect, expressing that objects in the neighbourhood of the target also contribute to the detected radiance. An equation for the radiance detected at the satellite is given by

$$\pi L_s = \pi L_p + E_{tot}\, r_t\, T \quad , \tag{1}$$

where L_s = radiance at satellite
L_p = path radiance
E_{tot} = total irradiance on the target
r_t = target reflectance (assumed Lambertian)
T = target-satellite transmittance

In terms of four-stream theory the atmospheric effect is illustrated in figure 2, which is an example of a so-called flux interaction diagram.

In this diagram each incident flux is represented by a square and each exitant flux by a circle. Each arrow indicates the direction of flow and the associated quantity is a reflectance factor (ρ or r) or a transmittance factor (τ). The subscripts for the atmospheric quantities refer to the types of incident and exitant flux, i.e. *s* for direct solar flux, *d* for diffuse flux and *o* for flux in the observer's direction. For the earth's surface the subscripts *t* and *b* refer to target and background, respectively. At the interface atmosphere - earth's surface the downward fluxes at the bottom of the atmosphere are exitant from the atmosphere and incident to the earth's surface at the same time, and a similar situation holds for the upward fluxes. In figure 2 dashed lines are used to express these identities. Next to the dashed lines the different contributions at ground level are mentioned. The transfer equations associated with figure 2 are the following:

$$E_s(\mathrm{b}) = \tau_{ss}\, E_s(\mathrm{t}) \quad , \tag{2a}$$
$$E^-(\mathrm{b}) = \tau_{sd}\, E_s(\mathrm{t}) + \rho_{dd}\, E^+(\mathrm{b}) \quad , \tag{2b}$$
$$E^+(\mathrm{b}) = r_b\, [E_s(\mathrm{b}) + E^-(\mathrm{b})] \quad , \tag{2c}$$
$$E_o(\mathrm{b}) = r_t\, [E_s(\mathrm{b}) + E^-(\mathrm{b})] \quad , \tag{2d}$$
$$E_o(\mathrm{t}) = \rho_{so}\, E_s(\mathrm{t}) + \tau_{do}\, E^+(\mathrm{b}) + \tau_{oo}\, E_o(\mathrm{b}) \quad , \tag{2e}$$

where (b) and (t) indicate the bottom and the top of the atmosphere. From equations (2b) and (2c) one finds the diffuse fluxes at the surface as

$E^{-}(b) = E_s(t)\ (\tau_{sd} + \tau_{ss}\ r_b\ \rho_{dd})\ /\ (1 - r_b\ \rho_{dd})$, and
$E^{+}(b) = E_s(t)\ (\tau_{ss} + \tau_{sd})\ r_b\ /\ (1 - r_b\ \rho_{dd})$

The total flux incident on the surface $E_{tot} = E_s(b) + E^{-}(b) = E_{sun} + E_{sky}$ is given by

$E_{tot} = E_s(t)\ (\tau_{ss} + \tau_{sd})\ /\ (1 - r_b\ \rho_{dd})$, and for $E_o(t)$,

which is the radiance in the observer's direction multiplied by π, one finds

$$E_o(t) = \pi L_s = E_s(t) \left[\rho_{so} + \frac{\tau_{ss} + \tau_{sd}}{1 - r_b\ \rho_{dd}} \left(r_b\ \tau_{do} + r_t\ \tau_{oo} \right) \right] \quad . \tag{3}$$

From comparison with Eq. (1) it follows that the path radiance can be found from

$\pi L_p = E_s(t)\ \rho_{so} + E_{tot}\ r_b\ \tau_{do}$, and that $T = \tau_{oo}$.

$E_s(t)$ equals $E_s^o \cos \theta_s$, where E_s^o is the extraterrestrial solar (spectral) irradiance on a plane perpendicular to the sunrays, and θ_s is the solar zenith angle. Apart form the influence of the distance sun-earth during the year, E_s^o can be assumed constant. The ratio $\pi L_s\ /\ E_s(t)$ is the planetary reflectance r_p.
The above description of the atmospheric effect is restricted to the case of a laterally homogeneous atmosphere over a surface for which both the target observed and the background act like Lambertian reflectors. As in general the background is not a homogeneous surface with a constant reflectance, r_b should be considered an average reflectance over some neighbourhood around the target.

3 Extinction and scattering coefficients of the atmosphere

Because of the spherical shape of the particles, and if not, their random orientation, the atmosphere is an isotropic medium, which means that the interception coefficient β is independent of the direction of the incident radiation. In this case the extinction coefficients for the fluxes E_s, E_o and the couple (E^-, E^+) are given by

$$k = \beta / \mu_s \; ; \quad K = \beta / \mu_o \; ; \quad \kappa = 2\beta \quad ,$$

where $\mu_s = |\cos \theta_s|$ and $\mu_o = |\cos \theta_o|$.

The scattering of incident light in the atmosphere is primarily described by the scattering phase function $p(\delta)$ for the angular distribution, and by the single scattering albedo ω for the relative amount of scattering. In the atmosphere nearly all the intercepted light is scattered, so ω is usually close to one.
For the angular distribution one makes the distinction between Rayleigh-scattering by air molecules and Mie-scattering by aerosol particles with a size comparable to the wavelength of the radiation. For Rayleigh-scattering the phase function can be approximated as

$$p_R(\delta) = \frac{3}{4} (1 + \cos^2 \delta) \quad ,$$

where δ is the scattering angle, i.e. the angle between the incident and the exitant ray.
Mie-scattering depends on the particle size distribution, the wavelength and the complex index of refraction of the material (cf. Deirmendjian, 1969 and De Haan, 1987). Extensions of Mie-theory to non-spherical particles are discussed in De Haan (1987) and Stammes (1989). In general, the phase function of aerosols is highly peaked in the forward direction (the aureole region) and more or less oscillatory around the backward direction (the glory region), especially if the material is non-absorbing. Figure 3 shows the Rayleigh phase function together with an example of Mie-scattering at a few wavelengths (water Haze M (maritime type) from Deirmendjian, 1969). From this it will be clear that the aerosol phase function $p_A(\delta)$ cannot be expressed by a simple function like the one for Rayleigh scattering.
The bidirectional scattering coefficient w is given by

$$w = \frac{\omega \beta p(\delta)}{4 \mu_s \mu_o} \quad , \text{ which holds for a single type of scattering.}$$

For a mixture of Rayleigh-scattering and aerosol-scattering it is formed by a linear combination as

$$w = \frac{\omega_R \beta_R p_R(\delta) + \omega_A \beta_A p_A(\delta)}{4 \mu_s \mu_o} \quad ,$$

where ω_R is the single scattering albedo for the Rayleigh case and can be taken equal to one. The subscripts *R* and *A* refer to Rayleigh and aerosol. Four-stream radiative transfer in the atmosphere (or any other scattering medium) is described by the matrix differential equation

$$\frac{\mathrm{d}}{\mathrm{d}z}\begin{pmatrix} E_s \\ E^- \\ E^+ \\ E_o \end{pmatrix} = \begin{pmatrix} k & & & \\ -s' & (\kappa - \sigma') & -\sigma & \\ s & \sigma & -(\kappa - \sigma') & \\ w & v & v' & -K \end{pmatrix}\begin{pmatrix} E_s \\ E^- \\ E^+ \\ E_o \end{pmatrix} \quad , \qquad (4)$$

in which *w* is as given above and the extinction coefficients *k*, *K*, and κ for a mixture of Rayleigh and aerosol scattering are given by

$$k = (\beta_R + \beta_A)/\mu_s \quad , \quad K = (\beta_R + \beta_A)/\mu_o \quad , \quad \kappa = 2(\beta_R + \beta_A) \quad .$$

The remaining scattering coefficients are all found by integration of *w* over the upper and lower hemisphere, i.e.

$$\pi s' = \int_{-2\pi} w \mu_o \, \mathrm{d}\Omega_o \quad , \quad \pi s = \int_{+2\pi} w \mu_o \, \mathrm{d}\Omega_o \quad ,$$

$$\pi v' = \int_{-2\pi} w \mu_s \, \mathrm{d}\Omega_s \quad , \quad \pi v = \int_{+2\pi} w \mu_s \, \mathrm{d}\Omega_s \quad ,$$

$$\pi \sigma' = \int_{+2\pi} s' \mu_s \, \mathrm{d}\Omega_s = \int_{+2\pi} v' \mu_o \, \mathrm{d}\Omega_o \quad , \quad \pi \sigma = \int_{+2\pi} s \mu_s \, \mathrm{d}\Omega_s = \int_{+2\pi} v \mu_o \, \mathrm{d}\Omega_o \quad ,$$

where $(-2\pi,+2\pi)$ indicates integration over the (lower, upper) hemisphere.

For Rayleigh scattering the integration of the phase function over one hemisphere gives always as a result 2π, half of the spherical integral. For the aerosol phase function this is not the case. Integration over the backward hemisphere (i.e. the upper hemisphere if $\mu_s = 1$ or $\theta_s = 0$) gives

the so-called backscattering efficiency η_A as

$$\eta_A = \frac{1}{4\pi} \int_0^{2\pi} \int_0^1 p\,(\mu_s = 1,\ \mu_o,\ \varphi_o)\ \mathrm{d}\mu_o\ \mathrm{d}\varphi_o \quad .$$

For most aerosol types η_A is of the order of 0.05, so 95 percent is scattered into the forward hemisphere.
Approximated values of the above scattering coefficients can now be found by assuming that always a fraction η_A of the incident flux is scattered into the hemisphere of incidence and a fraction $1-\eta_A$ into the opposite hemisphere. This gives

$$s' = \left[\tfrac{1}{2}\,\beta_R + \omega_A\,(1-\eta_A)\,\beta_A \right] / \mu_s \quad , \quad s = \left[\tfrac{1}{2}\,\beta_R + \omega_A\,\eta_A\,\beta_A \right] / \mu_s \quad ,$$

$$v' = \left[\tfrac{1}{2}\,\beta_R + \omega_A\,(1-\eta_A)\,\beta_A \right] / \mu_o \quad , \quad v = \left[\tfrac{1}{2}\,\beta_R + \omega_A\,\eta_A\,\beta_A \right] / \mu_o \quad ,$$

$$\sigma' = \beta_R + 2\,\omega_A\,(1-\eta_A)\,\beta_A \quad , \quad \sigma = \beta_R + 2\,\omega_A\,\eta_A\,\beta_A \quad ,$$

in which ω_R was assumed to be equal to one.

The combination $(\kappa - \sigma')$ in Eq. (4) is called the attenuation coefficient *a*, and is given by

$$a = \beta_R + 2\left[\,1 - \omega_A\,(1-\eta_A)\,\right]\beta_A \quad .$$

For the solution of Eq. (4) it is first assumed that the result will not depend much on the profiles of β_R and β_A as a function of the height *h* in the atmosphere. This is equivalent to assuming that the atmosphere forms a homogeneous mixture of Rayleigh and aerosol scattering, with associate optical thicknesses b_R and b_A , respectively. These are defined by

$$b_R = \int_0^\infty \beta_R(h)\,\mathrm{d}h \quad \text{and} \quad b_A = \int_0^\infty \beta_A(h)\,\mathrm{d}h \quad .$$

Assigning an arbitrary height *H* to the homogeneous atmospheric layer now gives the equivalent average interception coefficients β_R' and β_A' as

$$\beta_R' = b_R / H \quad \text{and} \quad \beta_A' = b_A / H \quad .$$

These can be used instead of β_R and β_A for the definition of the extinction and scattering coefficients. However, as the actual height is irrelevant for the solution of Eq. (4), one can just

as well take $H = 1$, so that $\beta_R' = b_R$ and $\beta_A' = b_A$. When Eq. (4) is written as $\frac{d}{dz}\boldsymbol{E} = \boldsymbol{M}'\boldsymbol{E}$, where $\boldsymbol{M}'$ is the matrix of coefficients with use of β_R' and β_A' , the concept of relative optical height is introduced as follows:

$$\text{Writing } d\boldsymbol{E} = \boldsymbol{M}'\boldsymbol{E}\,dz = \frac{\boldsymbol{M}}{H}\boldsymbol{E}\,dz = \boldsymbol{M}\boldsymbol{E}\frac{dz}{H} = \boldsymbol{M}\boldsymbol{E}\,dx \quad ,$$

where $\boldsymbol{M}$ is the matrix of coefficients for $H = 1$, leads to the replacement of the z co-ordinate by the relative optical height $x = z / H$. The range of x is also arbitrary, but it appears convenient if one takes $x = 0$ for the top and $x = -1$ for the bottom of the layer. This means that $x = (z\text{-}H) / H$. One can now write

$$\frac{d}{dx}\begin{pmatrix} E_s \\ E^- \\ E^+ \\ E_o \end{pmatrix} = \begin{pmatrix} k & & & \\ -s' & a & -\sigma & \\ s & \sigma & -a & \\ w & v & v' & -K \end{pmatrix}\begin{pmatrix} E_s \\ E^- \\ E^+ \\ E_o \end{pmatrix} \quad , \tag{5}$$

where x runs from -1 to 0 , and

$$k = (b_R + b_A)/\mu_s \quad ; \quad K = (b_R + b_A)/\mu_o \quad ;$$

$$w = \left[\, b_R\, p_R(\delta) + \omega_A\, b_A\, p_A(\delta) \,\right]/(4\,\mu_s\,\mu_o) \quad ;$$

$$s' = \left[\, \tfrac{1}{2}\, b_R + \omega_A\,(1 - \eta_A)\, b_A \,\right]/\mu_s \quad ; \quad s = \left[\, \tfrac{1}{2}\, b_R + \omega_A\,\eta_A\, b_R \,\right]/\mu_s$$

$$v' = \left[\, \tfrac{1}{2}\, b_R + \omega_A\,(1 - \eta_A)\, b_A \,\right]/\mu_o \quad ; \quad v = \left[\, \tfrac{1}{2}\, b_R + \omega_A\,\eta_A\, b_R \,\right]/\mu_o$$

$$a = b_R + 2\left[\, 1 - \omega_A\,(1 - \eta_A) \,\right] b_A \quad ; \quad \sigma = b_R + 2\,\omega_A\,\eta_A\, b_A$$

To the coefficients k, K and a can be added contributions due to gaseous absorption (for instance by water vapour) in the atmosphere. If the optical thickness associated with this absorption is called b_G, then these extra contributions are equal to b_G / μ_s , b_G / μ_o and $2b_G$, respectively. The solution of Eq. (5) can be expressed in matrix-vector form as

$$\begin{pmatrix} E_s\,(-1) \\ E^-\,(-1) \\ E^+\,(0) \\ E_o\,(0) \end{pmatrix} = \begin{pmatrix} \tau_{ss} & & & \\ \tau_{sd} & \tau_{dd} & \rho_{dd} & \\ \rho_{sd} & \rho_{dd} & \tau_{dd} & \\ \rho_{so} & \rho_{do} & \tau_{do} & \tau_{oo} \end{pmatrix}\begin{pmatrix} E_s\,(0) \\ E^-\,(0) \\ E^+\,(-1) \\ E_o\,(-1) \end{pmatrix} \quad , \tag{6}$$

in which the nine reflectance and transmittance factors are functions of the extinction and scattering coefficients as defined above. In Verhoef (1985) it was shown that these functions are rather simple, for instance

$$\tau_{ss} = e^{-k} \quad , \quad \tau_{oo} = e^{-K} \quad ,$$

$$\rho_{dd} = \frac{e^{m} - e^{-m}}{r_{\infty}^{-1} e^{m} - r_{\infty} e^{-m}} \quad , \quad \tau_{dd} = \frac{r_{\infty}^{-1} - r_{\infty}}{r_{\infty}^{-1} e^{m} - r_{\infty} e^{-m}} \quad ,$$

where $m = \sqrt{a^2 - \sigma^2}$ and $r_{\infty} = (a - m) / \sigma$.

Here, ρ_{dd} and τ_{dd} are equal to corresponding expressions of the Kubelka-Munk two-stream theory.

A special case, but not uncommon for atmospheric scattering, is the one encountered if $\omega_A = 1$ and $b_G = 0$ (no absorption at all). In this case $a = \sigma$, so $m = 0$, and ρ_{dd} and τ_{dd} become indeterminate if calculated according to the given expressions. This singularity can be removed if the limits for $m \rightarrow 0$ are taken, which gives

$$\lim_{m \to 0} \rho_{dd} = \frac{\sigma}{\sigma + 1} \quad \text{and} \quad \lim_{m \to 0} \tau_{dd} = \frac{1}{\sigma + 1} \quad .$$

The sum of both equals one, which is consistent with the absence of any absorption in the atmosphere.

4 Model implementation aspects

Of the nine reflectance and transmittance factors of Eq. (6), only six are needed for the determination of the atmospheric effect, namely the reflectance factors ρ_{so} and ρ_{dd} , and the transmittance factors τ_{ss} , τ_{sd} , τ_{do} and τ_{oo} , as can be seen in figure 2. These parameters describe the effects of Rayleigh scattering, scattering by aerosols and, possibly, absorption by gases like water vapour. However, absorption by ozone gas takes place mainly at altitudes of 20 to 25 km, well above the layer where the above mentioned processes are concentrated. Therefore, it is better to incorporate ozone absorption into the model by adding a separate layer at the top of the tropospheric layer. In this 'ozone layer' only absorption is supposed to take place, no scattering. The transmittance factors associated with absorption by ozone are symbolized as T_{sO3} and T_{oO3} and equal to

$$T_{s\,O3} = e^{-b_{O3}/\mu_s} \quad \text{and} \quad T_{o\,O3} = e^{-b_{O3}/\mu_o} \quad ,$$

where b_{O3} is the optical thickness due to ozone absorption. The reflectance and transmittance factors of the complete atmosphere should now be modified as

$$\rho_{so}^{\,*} = T_{s\,O3}\,\rho_{so}\,T_{o\,O3} \quad ; \quad \tau_{ss}^{\,*} = T_{s\,O3}\,\tau_{ss} \quad ; \quad \tau_{sd}^{\,*} = T_{s\,O3}\,\tau_{sd}$$

$$\tau_{do}^{\,*} = \tau_{do}\,T_{o\,O3} \quad ; \quad \tau_{oo}^{\,*} = \tau_{oo}\,T_{o\,O3}$$

As ρ_{dd} in the description of the atmospheric effect only plays the role of a spherical albedo at the bottom of the atmosphere, it does not need to be modified.
Values of b_{O3} at several wavelengths can be found in the literature. Apart from the well-known strong absorption of ultraviolet light by ozone, in the visible some additional absorption takes place, with a maximum at about 600 nm, where b_{O3} is of the order of 0.04 (cf. Elterman, 1970).

The optical thickness associated with Rayleigh scattering, b_R, depends strongly on the wavelength. According to Elterman (1970) it can be approximated by

$$b_R = 0.0987 \left(\frac{\lambda}{550} \right)^{-4.06} \quad , \text{ where } \lambda \text{ is the wavelength in nm.}$$

This means that halving the wavelength gives a more than 16-fold increase of the Rayleigh scattering optical thickness. The relationship given above holds for standard air pressure and temperature at sea level, but corrections for actual conditions can be carried out easily.

For aerosol scattering the dependence of b_A on wavelength is much weaker. If expressed as $b_A = \beta\lambda^{\alpha}$, where β and α are constants, the value of α, called the Ångström coefficient, is usually between −0.6 and −1.3 . However, this only applies to particle size distributions of a special type, namely the Junge-distribution, which is of the power law type. For the modified gamma distributions introduced by Deirmendjian (1969), the dependence on wavelength is different, although still smooth. Plotted on a log-log scale, Deirmendjian's curves are convex, with a negative slope which becomes more negative with increasing wavelength. This means that in this case α is not a constant, but itself a function of the wavelength. For the atmospheric correction model developed at NLR by the author, one of Deirmendjian's tabulated aerosol phase functions, namely the one for water Haze M (maritime type), was selected as a prototype for the representation of aerosol scattering behaviour in general. This function is tabulated at 34 values of the scattering angle δ and at a number of wavelengths in the range from 450 to 2250 nm. For the computation of $p_A(\delta)$ at arbitrary δ and λ, a cubic spline interpolation is carried out with respect to δ, and linear interpolation with respect to λ. The single scattering albedo ω_A for this type of aerosol is practically equal to one, but in the computer program smaller values of ω_A are allowed if so desired.

Water vapour in the atmosphere has absorption bands mainly in the infrared part of the spectrum, for instance at 930, 1150, 1400 and 1900 nm. Most optical remote sensing instruments avoid these bands, but the Landsat MSS scanner and the NOAA-AVHRR (advanced very high resolution radiometer) both have a spectral band that includes the absorption peak at 930 nm. The optical thickness associated with this is of the order of 0.1 (Saunders, 1988), but, like temperature and humidity, its variability is high, both spatially and temporarily. For instruments like the Landsat Thematic Mapper and the SPOT HRV the influence of water vapour absorption can probably be ignored in most cases.

Summarized, the greatest uncertainties in the atmospheric model are associated with the aerosol properties b_A, ω_A and $p_A(\delta)$, as these are highly variable or difficult to measure. Of these, b_A is the most important quantity because of its large influence on the extinction and scattering coefficients. The other two variables are less variable than b_A, since ω_A will mostly be rather close to one and $p_A(\delta)$ is roughly similar for different types of aerosol, especially in the range of δ involved in remote sensing missions ($\delta > \pi/2$). Therefore it appears not unreasonable to adopt representative samples of ω_A and $p_A(\delta)$, so that the only unknown left would be b_A.

5 Estimation of aerosol optical thickness

Several techniques can be applied to estimate the aerosol optical thickness b_A. The first, and the least reliable one, makes use of the parameter meteorological visual range, or visibility, which is defined as the horizontal distance at sea level over which the contrast at a wavelength of 550 nm is reduced to 2 percent of the one at zero distance. As this contrast reduction equals the direct horizontal transmittance T_{hor} , given by

$T_{hor} = e^{-\beta(0)d}$, where $\beta(0)$ is the interception coefficient at 550 nm in km^{-1} at sea level and d is the distance in km, one may put for $T_{hor} = 0.02$:

$0.02 = e^{-\beta(0)V}$, where V is the visibility in km, or

$\beta(0) = (\ln 50)/V$.

As $\beta(0)$ is the sum of the contributions due to Rayleigh scattering and aerosol scattering, one may write

$$\beta_R(0) + \beta_A(0) = (\ln 50)/V \quad , \quad \text{or} \quad \beta_A(0) = (\ln 50)/V - \beta_R(0) \quad .$$

From the literature, $\beta_R(0)$ at 550 nm is known to be equal to 0.0116, leading to V = 337 km if $\beta_A(0) = 0$. Such a high visibility is never found in reality at sea level. For cloudless atmospheres, a more realistic range for V is from 5 to 40 km. In that case $\beta_A(0)$ ranges from 0.086 at V = 40 km to 0.771 at V = 5 km.

A different measure of the state of the atmosphere is the turbidity factor T, which is defined as $T = (b_R + b_A) / b_R$, so it refers to the entire atmosphere, not to the situation at sea level, where V is based on.

Use of the visibility for estimation of b_A can only be carried out if it is known how β_A depends on the height in the atmosphere if $\beta_A(0)$ is given. A simple model of this profile was discussed in Sturm (1981) and consists of the following equations:

$$\beta_A(h) = \begin{cases} \beta_A(0)\, e^{-h/H1} & \text{if } h \le 5.5 \text{ km} \\ \beta_{A5.5} & \text{if } 5.5 \text{ km} < h < 18 \text{ km} \\ \beta_{A5.5}\, e^{(18-h)/H2} & \text{if } h \ge 18 \text{ km} \end{cases}$$

Together with that for Rayleigh scattering, this profile is illustrated in figure 4. For Rayleigh scattering $\beta_R(h) = \beta_R(0)\, e^{-h/H0}$, where $H0$ = 8.5155 km.

Here *H0*, *H1* and *H2* are so-called scale heights. Of these, *H0* and *H2* are considered constant, but *H1* is related to $\beta_A(0)$ by the requirement that $\beta_A(h)$ is continuous at h = 5.5 km, giving $\beta_A(0)\ e^{-5.5/H1} = \beta_{A5.5}$, or

$$H1 = 5.5 / \ln \left[\beta_A(0) / \beta_{A5.5} \right] \quad .$$

In Sturm's profile *H2* = 3.748 km and $\beta_{A5.5}$ at λ = 550 nm equals 0.0030765 km^{-1}. In that case the aerosol optical thickness of the layer above h = 5.5 km equals $\beta_{A5.5}$ (18 − 5.5 + *H2*) = 0.05. For the layer below h = 5.5 km one obtains an optical thickness of $[\beta_A(0) - \beta_{A5.5}]$ *H1*, so that the total optical thickness at λ = 550 nm is given by

$$b_A = \left[\beta_A(0) - \beta_{A5.5} \right] H1 + 0.05 \quad .$$

For visibilities V of 5 km and 40 km this gives b_A = 0.815 and b_A = 0.187, respectively. Corresponding values of the turbidity factor T are 9.26 and 2.89.
From the example above it appears that b_A at λ = 550 nm can be estimated if the visibility V is given and if one can be confident that the actual profile of β_A more or less matches the modelled profile as a function of the height. As shown by the example, the influence of the layer above h = 5.5 km is only small, so the greatest errors are expected to be associated with differences between actual and modelled profile in the lowest 5.5 km of the atmosphere. There is one particular situation in which the actual profile can be very different from the modelled one, namely in the case of an inversion layer in the atmosphere. In that case the normal decrease of the air temperature with height is interruped by a layer in which it is constant or increases. In such a situation a haze layer can develop at some height, while the atmosphere at the surface may still be relatively clear. It is obvious that in this case the visibility at ground level can only be a very poor indicator of the total aerosol optical thickness.
Other drawbacks of this technique are that visibility often is not measured but only visually estimated by a human observer, and that extrapolation of b_A to wavelengths other than λ = 550 nm is questionable.

The second technique uses model inversion, i.e. the estimation of model parameters from measurements, in order to estimate b_A. Some possibilities for this can be illustrated by means of figure 5, which shows the behaviour of some model output quantities as a function of b_A in the range from 0.0 to 1.0. All quantities shown are relative to the extraterrestrial solar irradiance, E_s^o, and the influence of the aerosol single scattering albedo ω_A on the results is demonstrated by showing results for ω_A = 1.0 and ω_A = 0.9. As appears from figure 5, measurement of E_{sun} gives the best estimate of b_A, since it is independent of ω_A. However, the value of E_s^o in the spectral band over which E_{sun} is measured must be known and E_{sun} must be measured with a

well-calibrated instrument, which sometimes can be problematic, as the usual absolute calibration accuracy is only of the order of ten percent. Measurement of both E_{sun} and E_{sky} , for instance by use of a Guzzi spectroradiometer (Veugen and Van Stokkom, 1985), can give good estimates of both b_A and ω_A, provided the calibration is accurate. This instrument has a rotating band which periodically blocks the sunlight from entering the detector, so a continuous measurement of E_{tot} and E_{sky} during the day is possible. If the calibration is questionable, then one can still get fairly accurate results for b_A by taking the ratio E_{sky} / E_{tot} , since in that case the calibration error is cancelled, and the influence of ω_A on this ratio is much smaller than on E_{sky} and E_{tot} separately.

Under favourable circumstances the ratio E_{sky} / E_{tot} can be measured from an image, for instance when a small cumulus cloud throws its shadow on a large homogeneous piece of land. The digital numbers of this object in the shadow and in the sunlit part can then be used for an estimate of the ratio E_{sky} / E_{tot} .

Another quantity that can be measured from an image is the atmospheric planetary reflectance $r_p(0)$, which is the planetary reflectance for zero ground reflectance. Under the condition that an object and its surroundings have a reflectance close to zero (for instance coniferous forest in the visible blue and red, or clear water in the near infrared), it may be assumed that the digital number *DN* for such a dark object can solely be attributed to atmospheric reflectance, so that after calibration of *DN* in units of reflectance an estimate of $r_p(0)$ is found. Provided the atmosphere over the scene is homogeneous, the lowest *DN* values of the scene can be associated with these dark objects, and the method based on this idea is therefore called the 'darkest pixel' method.

The potentials of both quantities E_{sky} / E_{tot} and $r_p(0)$ for estimation of b_A are illustrated in figures 6 and 7, respectively. Here, these quantities are shown as a function of b_A at 550 nm, under the assumption that $\alpha = -1.0$. Results are plotted for two wavelengths, namely $\lambda = 450$ nm (blue) and $\lambda = 700$ nm (red), and two values of ω_A, namely 0.9 and 1.0.

From figure 6 one may conclude that measurement of the ratio E_{sky} / E_{tot} can give a good estimate of the aerosol optical thickness b_A and that the influence of ω_A on this estimate is only moderate. Measurement of this quantity at two or more wavelengths can be used to estimate the Ångström-coefficient α as well.

As appears from figure 7, the relation between the atmospheric planetary reflectance $r_p(0)$ and b_A can also be used to estimate b_A, but the influence of ω_A on this relationship is considerable, especially at $\lambda = 450$ nm. Therefore it can be concluded that the 'darkest pixel method' cannot give good estimates of b_A, unless one has reason to believe that ω_A is very close to one, for instance when the aerosol is known to be of oceanic origin. Continental and urban aerosols usually contain more absorbing materials like soot and dust, and in that case ω_A can be much smaller. The strong wavelength-dependence of $r_p(0)$ suggests that the Ångström-coefficient can still be estimated fairly well from measurements of $r_p(0)$ at two or more wavelengths.

6 Atmospheric correction of Landsat Thematic Mapper images

On the basis of the material discussed in the previous chapters a procedure for the correction of atmospheric effects and calibration in units of ground reflectance has been developed for Landsat Thematic Mapper images. The Thematic Mapper instrument is an opto-mechanical multispectral scanner with 30 m ground resolution and has six spectral bands in the optical region and one in the thermal infrared (with 120 m ground resolution). The six optical spectral bands are called TM1 to TM5 plus TM7 (TM6 is the thermal infrared band) and are centered at wavelengths of 485, 560, 660, 830, 1650 and 2215 nm (visible, near and middle infrared), respectively.
Digital images acquired by the Landsat Thematic Mapper can be ordered from receiving stations in the USA, Europe and other locations.

Apart from the digital images, each data set contains also an extensive amount of auxiliary information, such as the scene location, time of acquisition, solar elevation angle and calibration constants. By means of the calibration data for each spectral band it is possible to calculate the detected radiances L_s from the digital number *DN* of an image pixel as

$$L_s = A0 + A1 * DN \quad , \tag{7}$$

where $A0$ = offset
$A1$ = gain factor .

The radiance detected at the satellite L_s can be related to the planetary reflectance r_p by

$$\pi L_s = r_p \, E_s^o \cos\theta_s / d^2 \quad , \tag{8}$$

where E_s^o is the extraterrestrial solar irradiance in the associate spectral band at a sun-earth distance of 1 Astronomical Unit (AU), and d is the actual distance in AU. The distance d is season-dependent, with a minimum on 3 January of 0.983 and a maximum on 2 July of 1.017, so that d^2 varies by about 7 percent. The average of d over a year is, by definition, equal to one. The planetary reflectance of an image pixel with digital number *DN* in a spectral band can be calculated by combining both equations, which gives

$$r_p = \frac{\pi \left(A0 + A1 * DN \right) d^2}{E_s^o \cos \theta_s} \quad . \tag{9}$$

It is important to note that E_s^o should be given in units which are compatible with those of $A0$ and $A1$. In this respect, the distributor of Landsat data in the USA, Eosat, specifies $A0$ and $A1$ in mW/(cm^2 sr μm), which means that the calibration constants are spectral radiances. In this

case the compatible unit for E_s^o is mW/(cm^2 μm). On the other hand, the European distributor Eurimage applies units of W/(m^2 sr), which refers to so-called in-band radiance, the integral of the spectral radiance over the width of the spectral band. In that case the compatible unit for E_s^o is W/m^2.

Besides the above complications, the user of Landsat TM data is also confronted with the fact that values of E_s^o for the TM bands are not given by the distributors, but have to be found in the specialist literature (cf. Markham and Barker, 1987). A good review of the difficulties associated with the calibration of Landsat TM data is given in Epema (1990). As a final remark it can be stated that much of the confusion could be avoided if the distributors would supply the users with alternative calibration constants *B0* and *B1* defined as $B0 = \pi\, A0 / E_s^o$ and $B1 = \pi\, A1 / E_s^o$. In that case,

$$r_p = (B0 + B1 * DN)\, d^2 / \cos\theta_s \quad , \tag{10}$$

and there can be no misunderstanding about the units of *B0* and *B1*, as they are dimensionless. In addition, the user would not have to consult other sources of information, as was the case with E_s^o .

According to Eq. (3) of chapter 2, the planetary reflectance r_p is given by

$$r_p = \rho_{so} + \frac{\tau_{ss} + \tau_{sd}}{1 - r_b\, \rho_{dd}} (r_b\, \tau_{do} + r_t\, \tau_{oo}) \quad , \tag{11}$$

where the atmospheric parameters ρ_{so} , ρ_{dd} , τ_{ss} , τ_{sd} , τ_{do} and τ_{oo} can be obtained from model calculations, r_b is the background reflectance and r_t is the target reflectance. Since the background reflectance r_b is not known a priori, in a first approximation it may be assumed that r_b equals r_t. Of course this can only be correct if the target is large enough. In that case,

$$r_p = \rho_{so} + \frac{T_1\, T_2\, r_t}{1 - r_t\, \rho_{dd}} \quad , \text{ where } T_1 = \tau_{ss} + \tau_{sd} \text{ and } T_2 = \tau_{oo} + \tau_{do} \quad .$$

Solution of r_t from this equation gives

$$r_t = \frac{r_p - \rho_{so}}{T_1 T_2 + (r_p - \rho_{so})\, \rho_{dd}} \quad . \tag{12}$$

So, for this simple atmospheric correction method it is only necessary to calculate r_p from *DN* using the calibration data, and to know the atmospheric parameters ρ_{so} , ρ_{dd} and the product T_1T_2 for each spectral band. As explained in the previous chapter, the most unknown quantity

for the determination of the atmospheric parameters is the aerosol optical thickness b_A. However, it was shown that b_A can be estimated from measured data of the ratio E_{sky} / E_{tot} or from values of the darkest pixel planetary reflectance $r_p(0)$ extracted from the image. In both cases model inversion is applied to estimate b_A. This is done by means of iteration, i.e. the input value b_A is varied until the calculated output quantity matches the measured value. If this technique is applied for two or more wavelengths, then the wavelength-dependence of b_A can be determined by means of the assumed relationship $b_A(\lambda) = \beta\lambda^{\alpha}$, or $\log b_A(\lambda) = \log \beta + \alpha \log \lambda$. Linear regression of $\log b_A(\lambda)$ against $\log \lambda$ thus provides least squares estimates of the parameters β and α. Subsequently, β and α can be applied in order to estimate $b_A(\lambda)$ in all the Thematic Mapper bands in the optical region, after which also ρ_{so} , ρ_{dd} and T_1T_2 can be calculated by means of the atmospheric model in all spectral bands.

With respect to the darkest pixel method it should be mentioned that the linear regression $\log b_A$ - $\log \lambda$ leads to a straight line (best fit) around which the model-inverted values b_A^* are scattered if more than two wavelengths were used, so that some points will lie above the regression line and some will lie under it. For the wavelengths at which b_A^* is under the regression line, application of the best fit value b_A in the calculation of the atmospheric parameters ρ_{so} , ρ_{dd} and T_1T_2 will result in an over-estimation of the atmospheric effect. Especially, ρ_{so} will be greater than the darkest pixel planetary reflectance $r_p(0)$ in that case, so that for the darkest pixels negative values of the target reflectance r_t would be computed. In order to avoid this, the regression line is lowered parallel to itself until it goes through the point having the largest difference between $\log b_A$ and $\log b_A^*$. In this way the Ångström coefficient α remains the same, but β is lowered to a new value β'. Next, the relationship $b_A(\lambda) = \beta'\lambda^{\alpha}$ is used for the estimation of ρ_{so} , ρ_{dd} and T_1T_2 by means of the model.

The actual correction of an image by means of equations (9) and (12) is carried out by means of a look-up table (LUT) for each spectral band. As Landsat TM images are 8 bit per band, each input pixel *DN* is in the range 0-255, so each LUT has 256 entries. If the corrected image is also encoded in 8 bits per band, and the corrected digital number is called *DN′*, then the correction is carried out by applying the operation *DN′* = LUT (*DN*) to each pixel in the image for each spectral band. As *DN′* represents a reflectance value in the range 0.0-1.0, it is necessary to specify a scale factor *s* which relates reflectance to digital number. This scale factor should be smaller than 256 in order to prevent overflow.
The entire procedure for atmospheric correction of a Landsat TM image is summarized below for the darkest pixel method:

1. Enter date $\rightarrow d^2$
   Enter θ_s
   Enter TM-calibration data file name

2. For two or more TM bands:
   Enter darkest pixel *DN*
   $DN \rightarrow r_p$ (calibration)
   Iterate b_A^* until ρ_{so} (model) $= r_p$
3. Linear regression $\log b_A^*$ vs. $\log \lambda$ $\rightarrow \log b_A = \log \beta + \alpha \log \lambda$
   Lower regression line $\rightarrow \log b_A = \log \beta' + \alpha \log \lambda$
4. For all TM bands:
   $b_A = \beta' \lambda^{\alpha}$
   model $\rightarrow \rho_{so}$, ρ_{dd} , $T_1 T_2$
5. Enter scale factor *s*
6. For all TM bands:
   For *DN* = 0,1,...,255:
      $DN \rightarrow r_p$ (calibration)
      $r_p \rightarrow r_t$ (atmospheric correction)
      LUT (*DN*) = $s * r_t$
   For all pixels:
      DN′ = LUT (*DN*)
7. End

For the method based on measurements of E_{sky} / E_{tot} the procedure is similar, except that step 2 consists of:

2. For two or more wavelengths:
   Enter measured E_{sky} / E_{tot}
   Iterate b_A^* until E_{sky} / E_{tot} (model) = E_{sky} / E_{tot} (measured)

Also, the lowering of the regression line in step 3 is omitted in this case.

For both methods of correction the computation time is neglible, mainly because the model is simple, the iteration converges rapidly and the look-up table operation used in the correction can be carried out very efficiently.

7 Validation results

Although in practice a true validation of an atmospheric model is a very difficult task because of the great number of parameters that would have to be measured, and no specific attempts have been initiated in this direction, the model and the correction methods based on it have been used in several projects, in all cases with the aim to improve the spectral characterization of objects on the ground and to facilitate multitemporal comparison.

In one project, described by Epema (1992), also in situ ground measurements of the reflectance were available, so that the performance of the correction method could be tested. In this case the method based on the ratio E_{sky} / E_{tot} was used in Tunesia, where this ratio was measured by shadowing a reference panel. The main conclusions were that for a Landsat TM image of April 1988 the correspondence between ground reflectances derived from the image and measured values was good (maximum relative error 10 percent), but for an image of December 1987 larger errors were observed. However, these could be attributed to water vapour absorption in TM bands 4, 5 and 7. After incorporating this water vapour absorption into the model the results improved significantly.

In another project (Verhoef, 1990) the darkest pixel method has been tested for images of the Flevoland area in The Netherlands, acquired in the summer of 1986. Some results of this exercise are discussed below.

Tables 1 and 2 summarize the numerical results of the model inversion and the computed correction constants for Landsat TM images of 16 June and 3 August 1986, respectively. In both cases, four TM bands were used for the estimation of b_A from darkest pixel digital numbers. Of these, TM1 (blue) and TM4 (near infrared) are the most reliable ones, since the darkest pixels in these bands most likely refer to objects having a reflectance very close to zero, such as coniferous forest in TM1 and clear water in TM4, which both are present in the images. In TM2 (green) and TM3 (red) the darkest objects probably still have a reflectance of the order of one percent, and this might lead to overestimation of b_A in these bands, as this small reflectance would wrongly be attributed to the atmospheric effect.

Therefore, the procedure was modified by allowing the specification of a small reflectance for the darkest object. In the tables these are indicated by r_t for the different spectral bands. The results of the linear regression log b_A vs. log λ are given by the parameters α and β, and the squared correlation coefficient R^2 and the root mean square error ε of b_A. For both dates a very good fit was found, as expressed by the high values of R^2 and the small values of ε. Also, the Ångström coefficient α is in the expected range of -0.6 to -1.3.

Comparing the results for both dates, there appears to be a large difference in the atmospheric turbidity, as evidenced by the difference in the aerosol optical thickness b_A , but this does not lead to very great differences in the correction constants ρ_{so} , T_1T_2 and ρ_{dd} . The reason for this is probably the fact that at shorter wavelengths Rayleigh scattering, which is constant, tends to

dominate the atmospheric effect, and that at the longer wavelengths the atmospheric effect is small anyway, except for possible effects due to water vapour absorption, as found by Epema. From the two atmospherically corrected and calibrated images, TM-derived spectral reflectance 'signatures' have been extracted for a number of different objects in order to evaluate the performance of the correction. The results are presented in figures 8 and 9. In both figures the solid lines refer to the 16 June image and the dashed lines to the 3 August image. In figure 8 also results of field spectrometer measurements for grass and sugar beet, as obtained during the NIWARS programme in 1973 (Bunnik, 1978), have been included for comparison. The TM-derived grass spectrum of 16 June appears to be very similar to the measured NIWARS spectrum of 1 August 1973. This difference in date is of no significance, however, as grass can be in any stage of development during the summer. For sugar beet one can safely assume that the growth stage on 3 August 1986 is similar to the one on 28 August 1973 so that the TM-derived spectrum of 3 August should be comparable with the NIWARS measurement. Especially for TM5 and TM7 correspondence is very good, so there is no evidence of water vapour absorption in these bands, like was found by Epema, as otherwise the reflectances in TM5 and TM7 would be significantly smaller than the measured values, and this is not the case. There is, however, a remarkable difference in TM2: the measured spectrum shows a pronounced peak in the reflectance in the green, whereas this peak in the TM-derived spectrum is much weaker. Two possible causes of this are 1) the band width of 85 nm associated with TM2, which could be too wide to resolve the green peak clearly, and 2) the adjacency effect, which tends to wash out spectral differences between a target and its surroundings. More evidence for the latter is found in figure 9, which shows TM-derived spectra of coniferous forest and other 'stable' objects like sand, an urban area and a small lake containing clear water. This evidence appears in the form a peak in the reflectance in TM4 for the small lake and the fact that the spectra of sand and clear water are wider apart on 3 August than on 16 June, which can be explained by a stronger adjacency effect on 16 June due to more haze in the atmosphere. Nevertheless, the performance of the atmospheric correction in terms of spectral characterization can be considered good, as the changes found for the stable objects between the two dates are relatively small.

8 Conclusions

A four-stream atmospheric radiative transfer model has been described which has been applied to the correction of Landsat Thematic Mapper images for atmospheric effects and the calibration in surface reflectance units.

The proposed method makes use of literature data and the darkest pixels in a scene in order to derive the aerosol optical thickness as the prime unknown quantity. This has the advantage that it is easy to implement the algorithm on an operational bases, since the necessary input is extracted from the image and further consists of usually available data like the calendar date and the solar elevation at the time of overpass. A disadvantage is that violation of the assumptions made leads to errors.

It has been demonstrated that application of this simple method of atmospheric correction gives satisfactory results in most cases. Samples of the surface reflectance extracted from the corrected images appear to correspond rather well with the results of reflectance measurements in the field. However, there are indications that in the infrared the absorption by water vapour in the atmosphere is sometimes underestimated and that for accurate results it might be worth considering a more advanced modelling of the adjacency-effect.

9 References

Bunnik, N.J.J., "The multispectral reflectance of shortwave radiation in relation with their morphological and optical properties", Thesis Agricultural University, Wageningen, 1978

Deirmendjian, D., "Electromagnetic scattering on spherical polydispersions", American Elsevier Publ. Co., New York, 1969

Elterman, L., "Vertical attenuation model with eight surface meteorological ranges 2 to 13 km", AFCRL, Bedford, Mass., NTIS-AD 707 488, 1970

Epema, G.F., "Determination of Planetary Reflectance for Landsat-5 Thematic Mapper Tapes Processed by Earthnet (Italy)", ESA Journal, Vol. 14, 1990

Epema, G.F., "Spectral reflectance in the Tunesian desert", Thesis Agricultural University, Wageningen, 1992

De Haan, J.F., "Effects of aerosols on the brightness and polarization of cloudless planetary atmospheres", Thesis Vrije Universiteit, Amsterdam, 1987

Markham, B.L., and Barker, J.L., "Thematic Mapper bandpass solar exo-atmospheric irradiances", Int. J. Rem. Sens., Vol. 8, No. 3, 517-523, 1987

Saunders, R.W., "The determination of broad band surface albedo from AVHRR visible and near infrared radiances", MET O 19 Branch Memorandum No. 96, Clarendon Lab., Oxford, 1988

Stammes, P., "Light scattering properties of aerosols and the radiation inside a planetary atmosphere", Thesis Vrije Universiteit, Amsterdam, 1989

Sturm, B., "The atmospheric correction of remotely sensed data and the quantitative determination of suspended matter in marine water surface layers", in: Remote Sensing in Meteorology, Oceanography and Hydrology, Ellis Horwood Ltd., Chicester, England, 1981

Verhoef, W., "Earth observation modelling based on layer scattering matrices", Rem. Sens. of Env. 17: 165-178, 1985

Verhoef, W., "Informatie-extractie uit multispectrale beelden met behulp van stralings-interactiemodellen", NLR TP 90243 L, 1990

Veugen, L.M.M, and Van Stokkom, H.T.C., "An atmospheric correction method using Guzzi-spectroradiometer data", in: Proc. 3rd Int. Coll. on Spectral Signatures of Objects in Rem. Sens., pp. 383-388, ESA SP-247, 1985

Table 1 Darkest pixel correction results for 16-06-1986

Sun-earth distance in AU : 1.01593661
Solar zenith angle (deg) : 33.7

TM	λ (nm)	Darkest pixel	r_p	r_t	b_R	b_{O3}	b_A^*	b_A
1	485	78	.115	.000	.165	.008	.745	.743
2	560	28	.083	.010	.092	.030	.681	.675
3	660	22	.060	.008	.047	.010	.619	.604
4	830	11	.033	.000	.019	.000	.518	.518

$\alpha = -.671$
$\beta = .458$
$R^2 = .995$
$\varepsilon = .007$

Correction constants:

TM	ρ_{so}	T_1T_2	ρ_{dd}
1	.1150	.7188	.2025
2	.0750	.7567	.1451
3	.0524	.8479	.1017
4	.0333	.9136	.0670
5	.0115	.9646	.0287
7	.0085	.9718	.0232

Table 2 Darkest pixel correction results for 03-08-1986

Sun-earth distance in AU : 1.01470556
Solar zenith angle (deg) : 39.6

TM	λ (nm)	Darkest pixel	r_p	r_t	b_R	b_{O3}	b_A^*	b_A
1	485	59	.093	.000	.165	.008	.457	.457
2	560	20	.063	.007	.092	.030	.406	.401
3	660	15	.043	.007	.047	.010	.348	.345
4	830	7	.020	.000	.019	.000	.218	.208

$\alpha = -.911$
$\beta = .236$
$R^2 = .999$
$\varepsilon = .003$

Correction constants:

TM	ρ_{so}	T_1T_2	ρ_{dd}
1	.0933	.7519	.1800
2	.0566	.7872	.1231
3	.0363	.8797	.0782
4	.0202	.9432	.0452
5	.0051	.9831	.0140
7	.0033	.9879	.0101

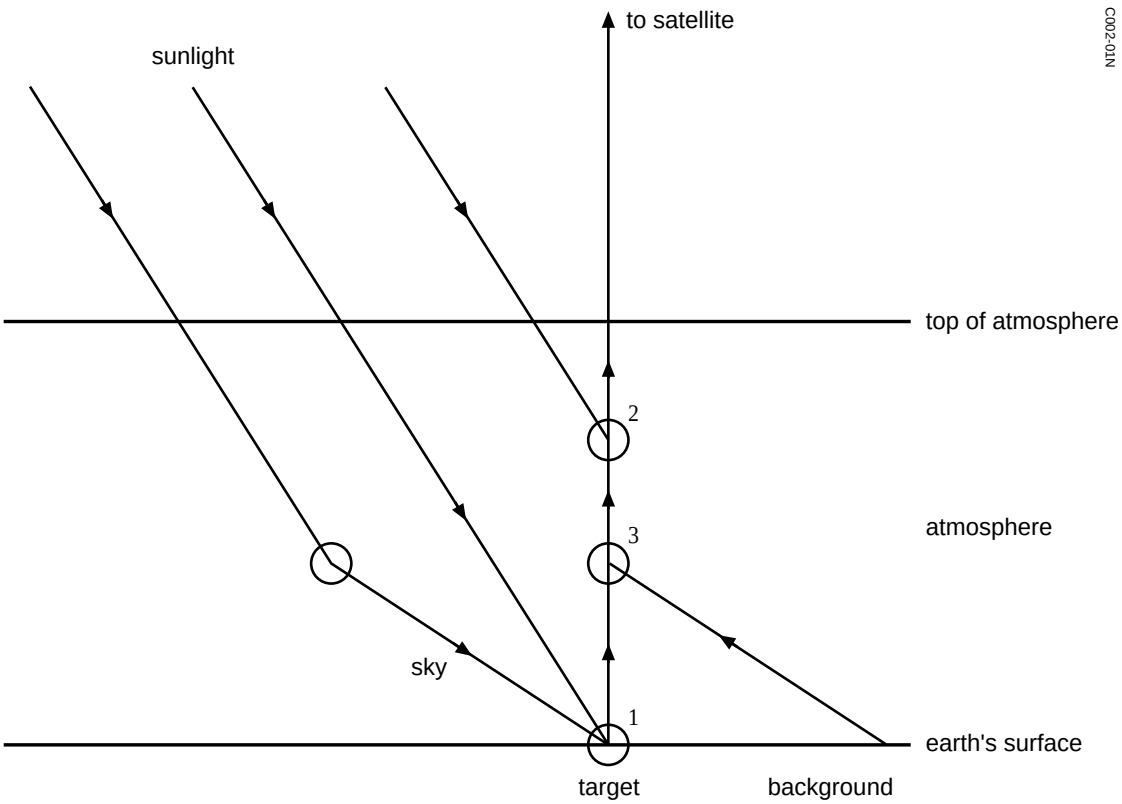

Fig. 1 Atmospheric effect on satellite observations of the earth

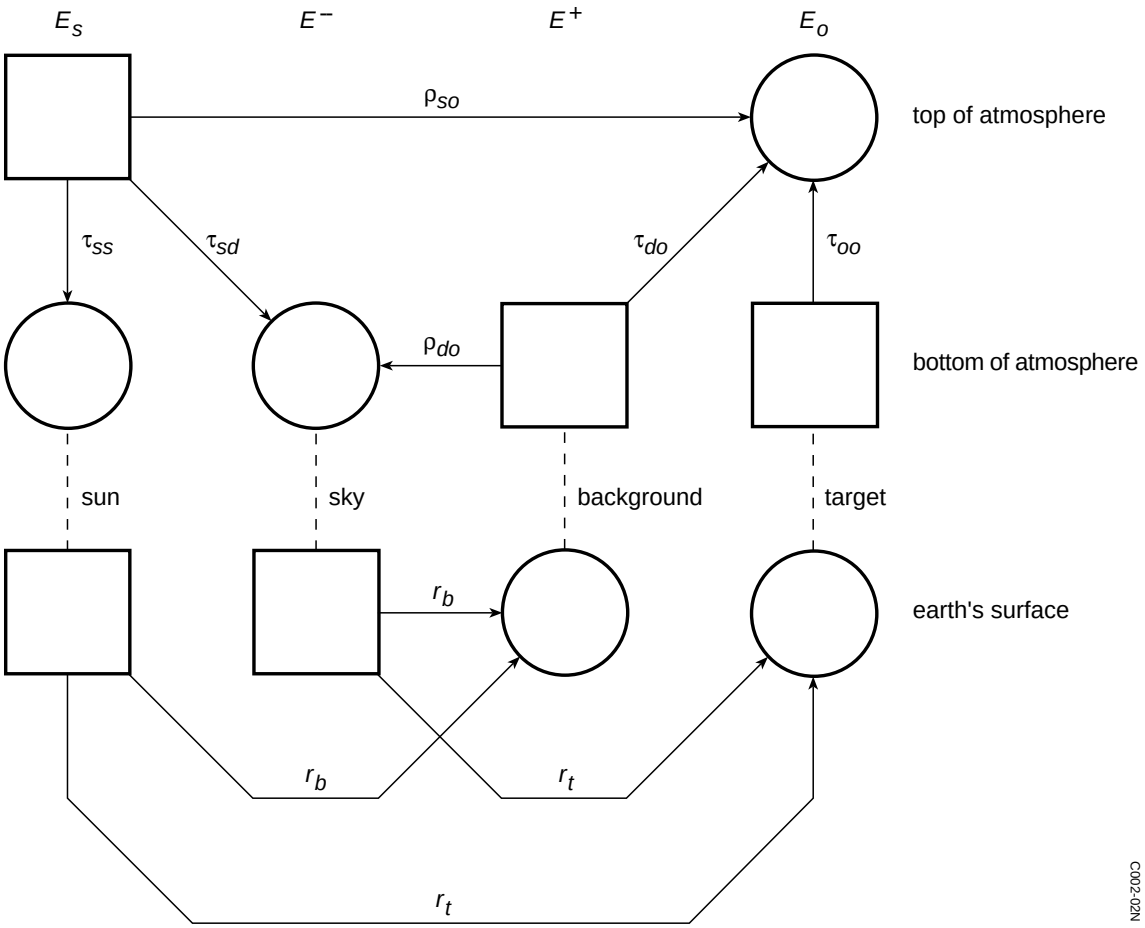

Fig. 2 Four-stream flux interaction diagram for the atmospheric effect

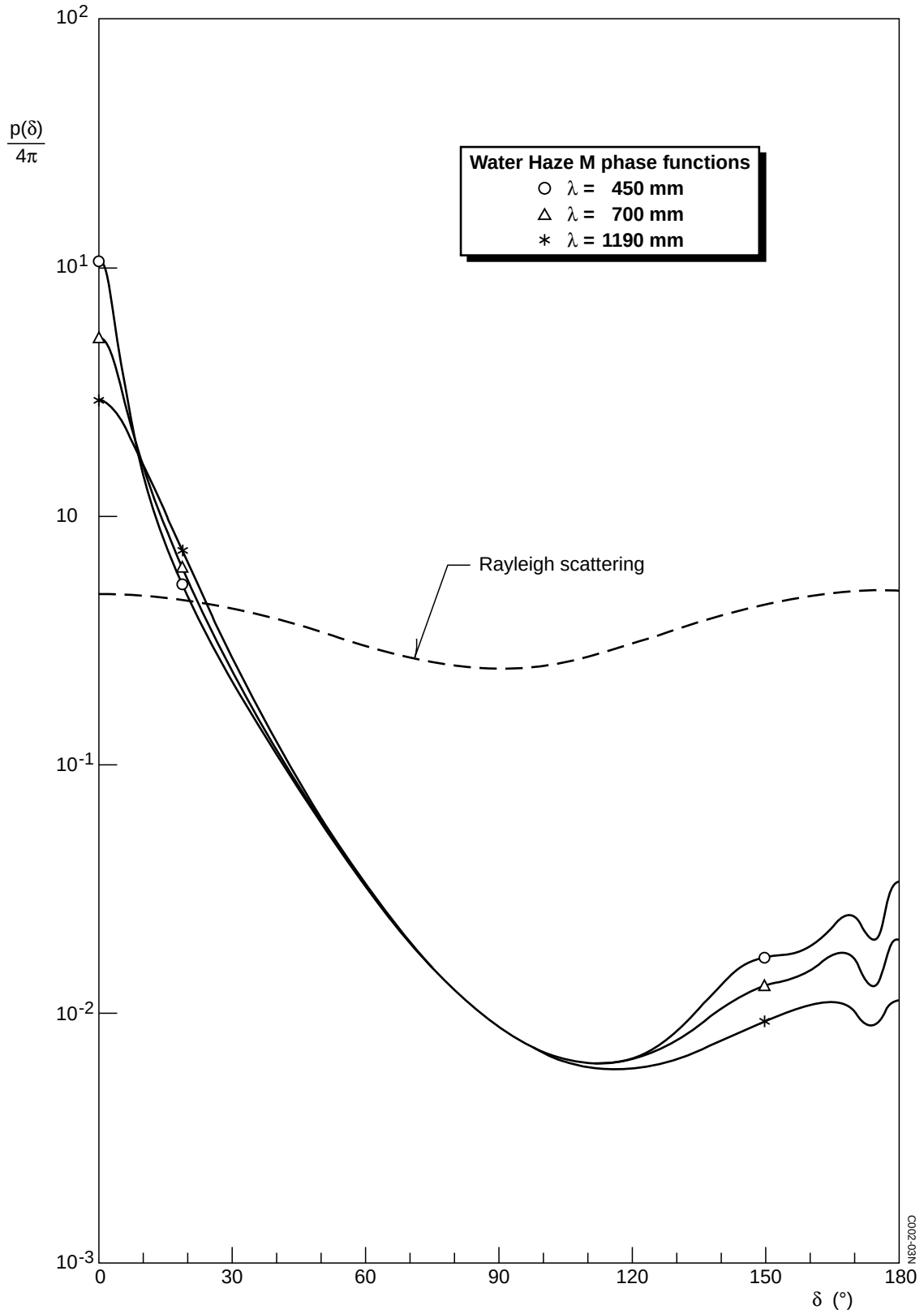

Fig. 3 Aerosol and Rayleigh scattering phase functions

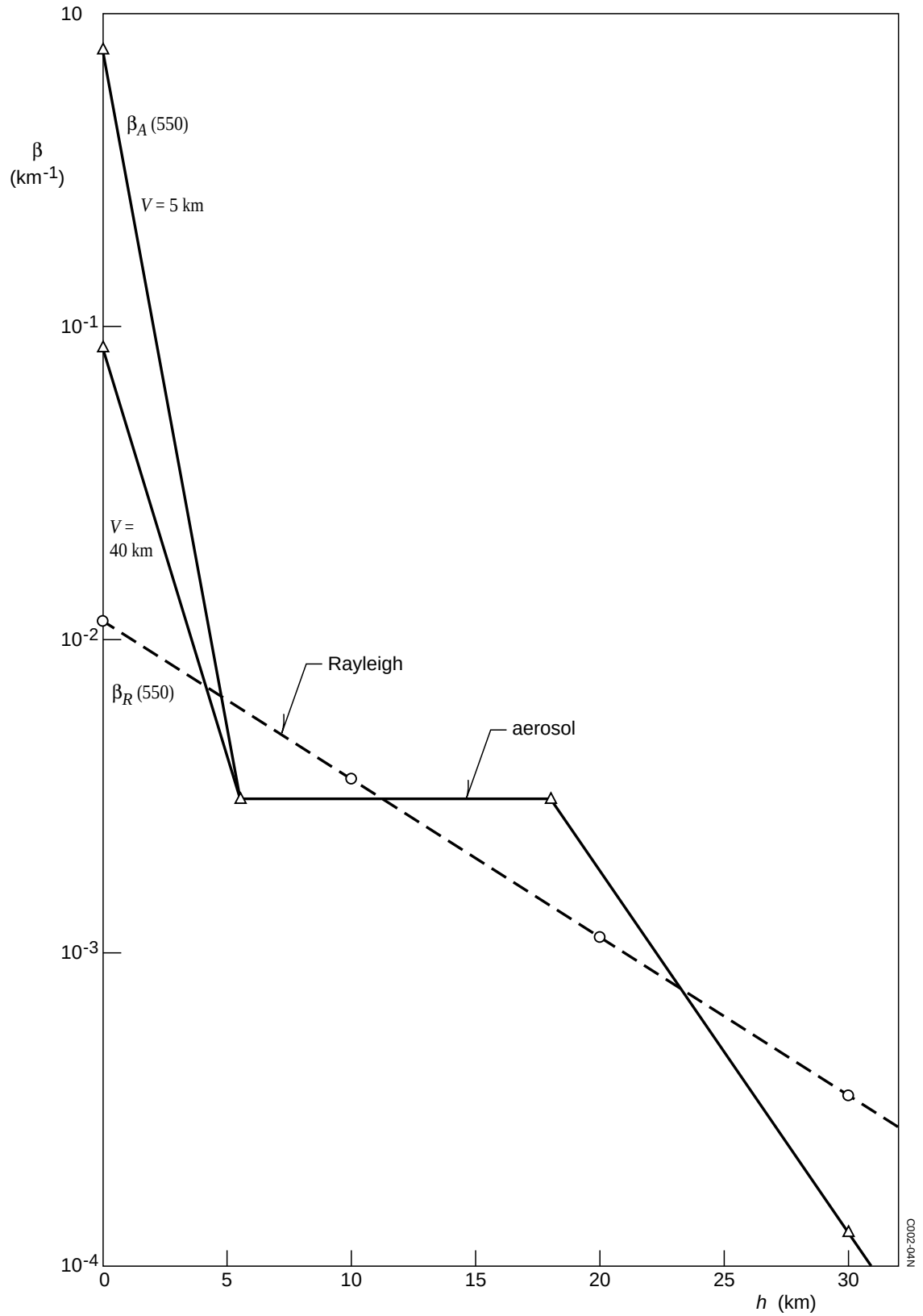

Fig. 4 Height profiles of the interception coefficients for aerosol and Rayleigh scattering, according to Sturm (1981)

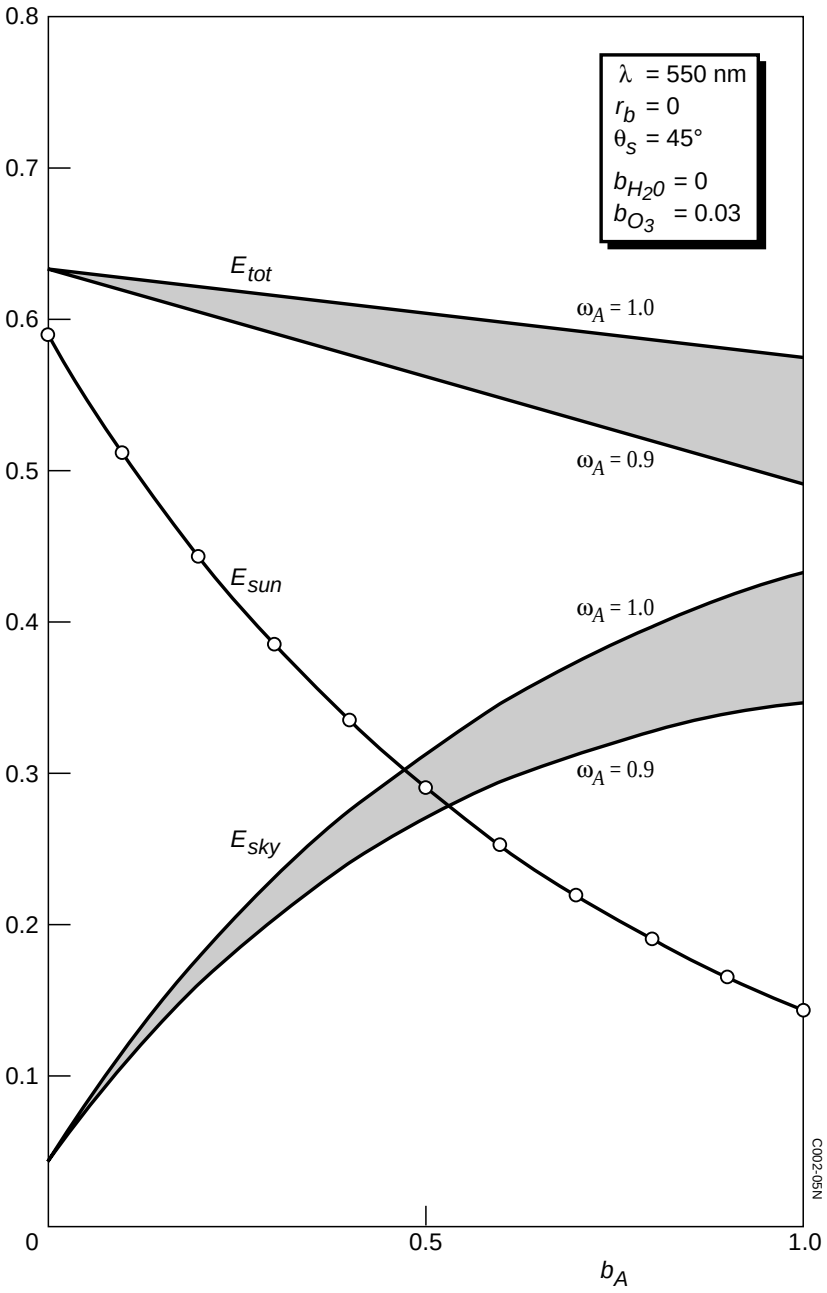

Fig. 5 Solar, sky and total irradiance at ground level (relative to E_s^0) as a function of b_A and ω_A at λ = 550 nm

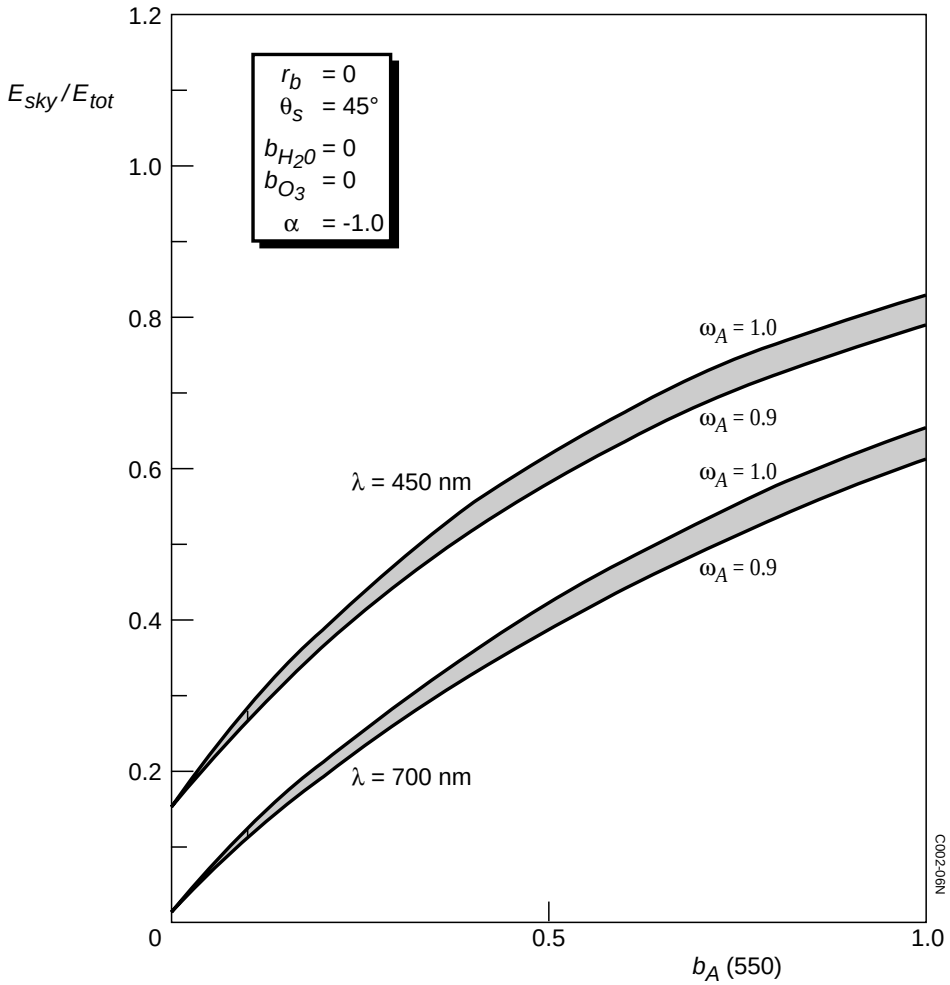

Fig. 6 The ratio E_{sky}/E_{tot} at λ = 450 nm and λ = 700 nm as a fucntion of b_A at λ = 550 nm for α = -1.0 and ω_A = 0.9 to 1.0

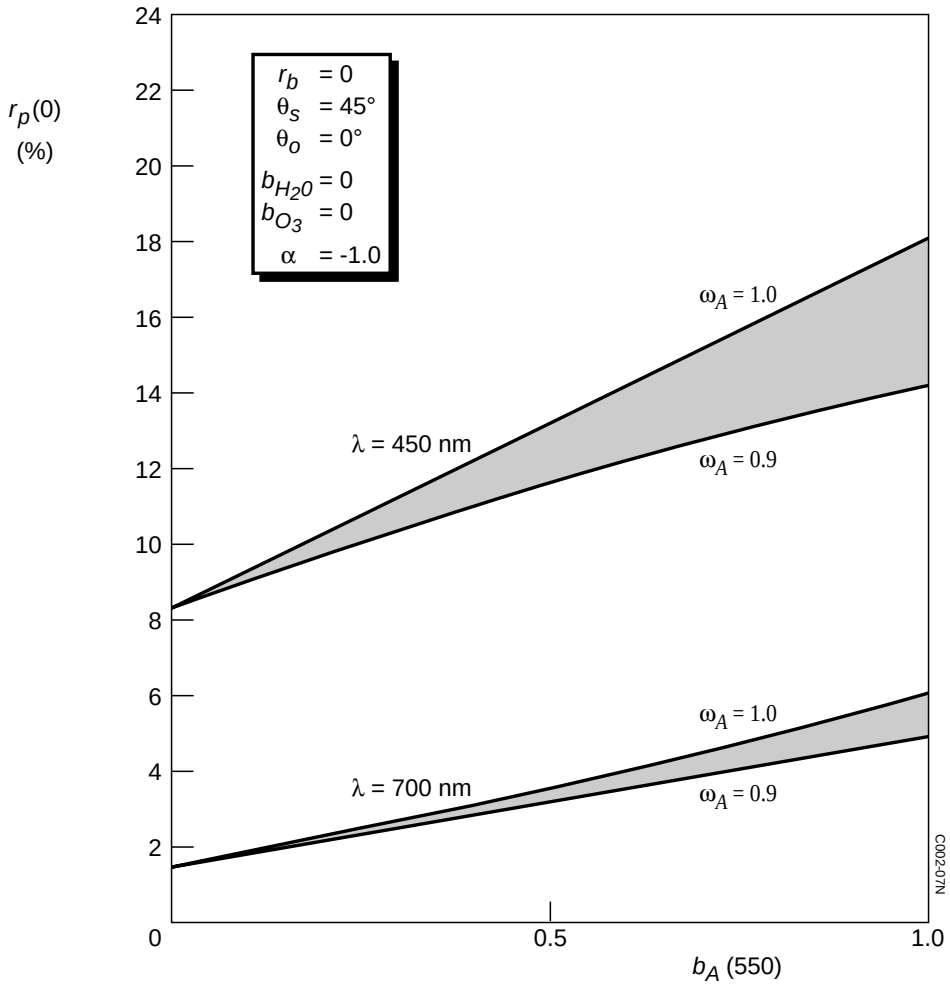

Fig. 7 The atmospheric planetary reflectance $r_p(0)$ at λ = 450 nm and λ = 700 nm as a fucntion of b_A at λ = 550 nm for α = -1.0 and ω_A = 0.9 to 1.0

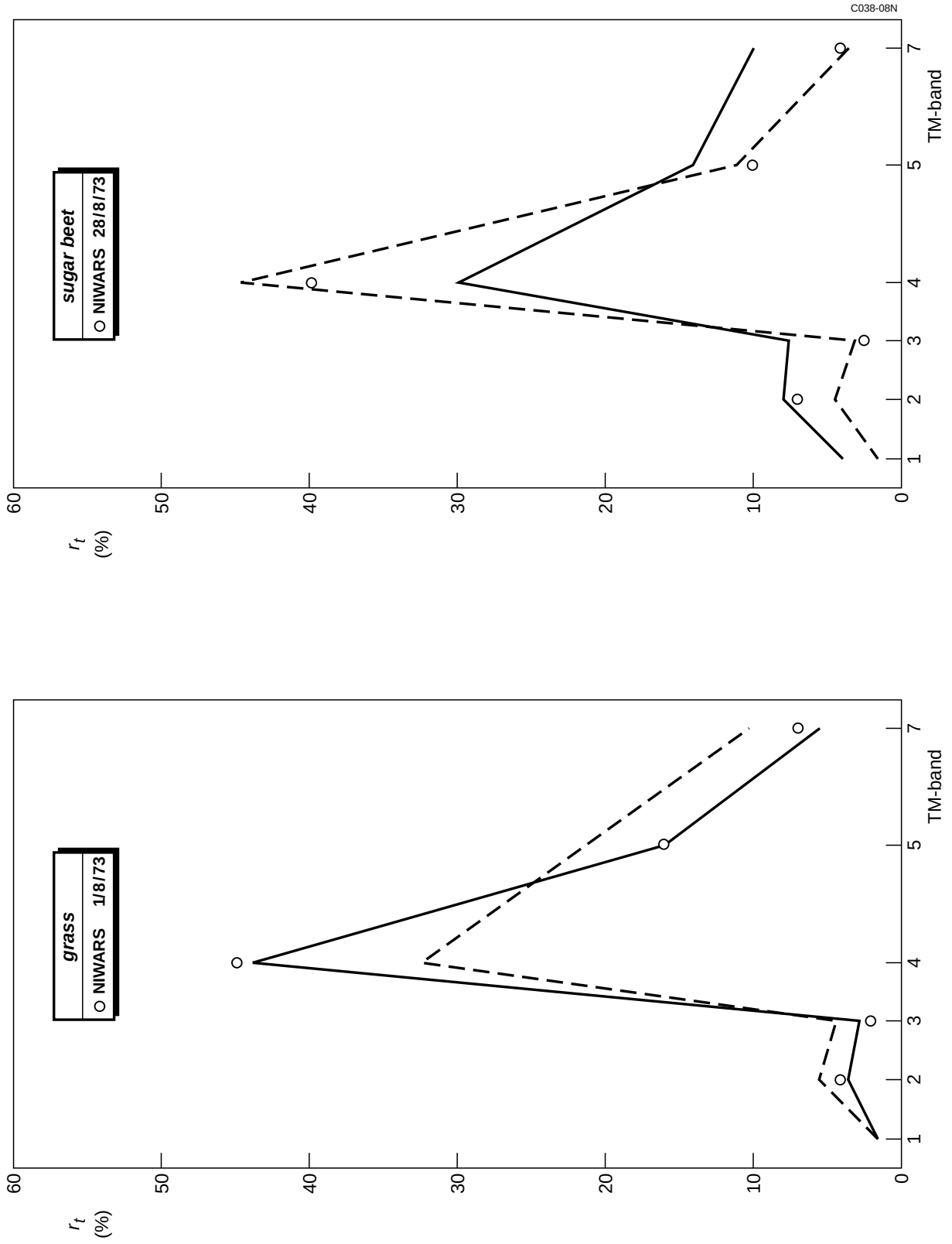

Fig. 8 TM-derived spectral reflectance for grass and sugar beet compared with NIWARS field spectrometer measurements in 1973 (Bunnik, 1978)

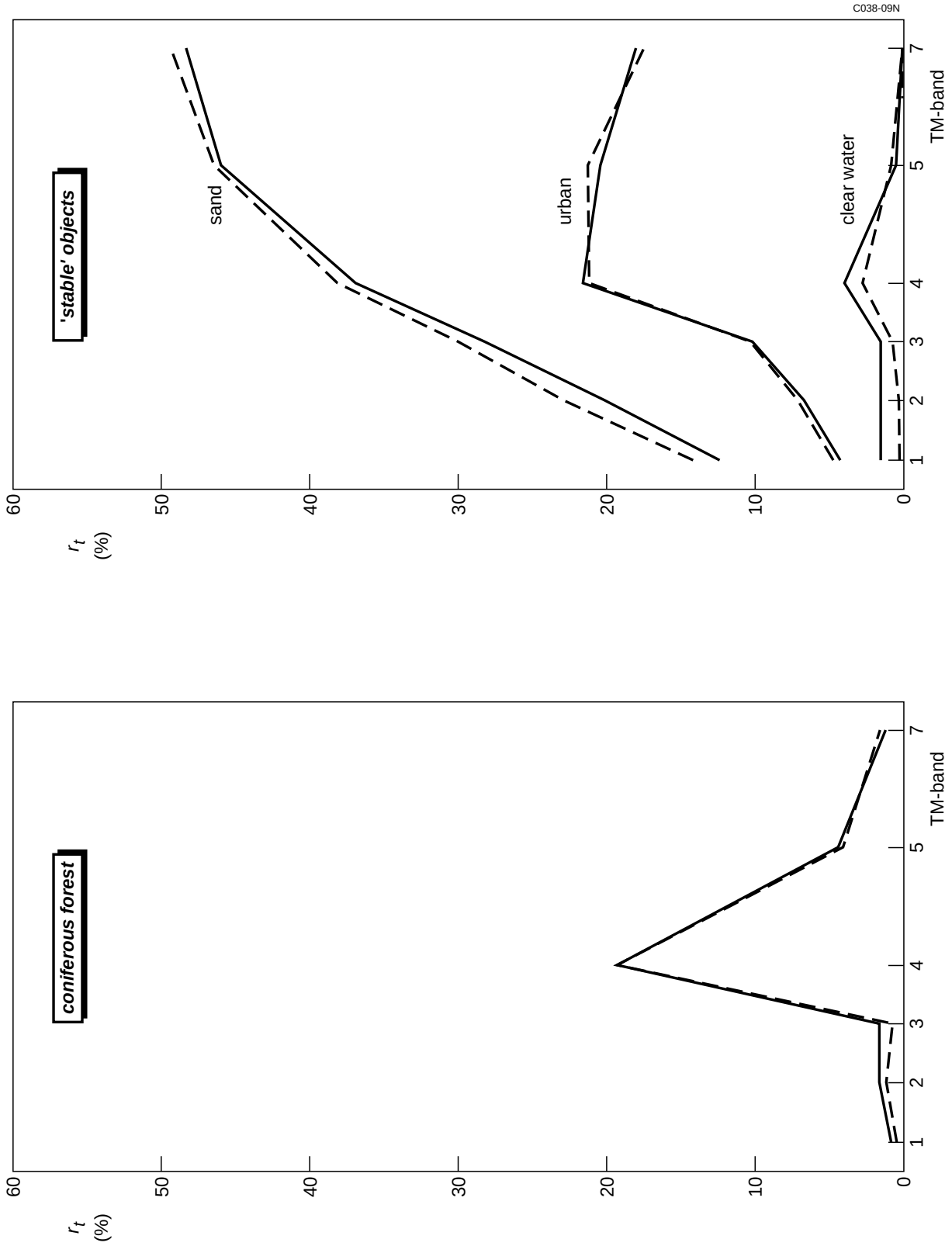

Fig. 9 TM-derived spectral reflectance of coniferous forest and other 'stable' objects